7-18-2019

Continuous Monitoring of Soil Nitrate Using a Miniature Sensor with Poly(3-octyl-thiophene) and Molybdenum Disulfide Nanocomposite

Md. Azahar Ali
Iowa State University

Xinran Wang
Iowa State University, xrwang@iastate.edu

Yuncong Chen
Iowa State University, yuncongc@iastate.edu

Yueyi Jiao
Iowa State University, jyymoone@iastate.edu

Navreet K. Mahal
Iowa State University, nmahal@iastate.edu
See next page for additional authors

Continuous Monitoring of Soil Nitrate Using a Miniature Sensor with Poly(3-octyl-thiophene) and Molybdenum Disulfide Nanocomposite

Abstract

There is an unmet need for improved fertilizer management in agriculture. Continuous monitoring of soil nitrate would address this need. This paper reports an all-solid-state miniature potentiometric soil sensor that works in direct contact with soils to monitor nitrate-nitrogen (NO3--N) in soil solution with parts-per-million (ppm) resolution. A working electrode is formed from a novel nanocomposite of poly(3-octyl-thiophene) and molybdenum disulfide (POT–MoS2) coated on a patterned Au electrode and covered with a nitrate-selective membrane using a robotic dispenser. The POT–MoS2 layer acts as an ion-to-electron transducing layer with high hydrophobicity and redox properties. The modification of the POT chain with MoS2 increases both conductivity and anion exchange, while minimizing the formation of a thin water layer at the interface between the Au electrode and the ion-selective membrane, which is notorious for solid-state potentiometric ion sensors. Therefore, the use of POT–MoS2 results in an improved sensitivity and selectivity of the working electrode. The reference electrode comprises a screen-printed silver/silver chloride (Ag/AgCl) electrode covered by a protonated Nafion layer to prevent chloride (Cl-) leaching in long-term measurements. This sensor was calibrated using both standard and extracted soil solutions, exhibiting a dynamic range that includes all concentrations relevant for agricultural applications (1–1500 ppm NO3--N). With the POT–MoS2 nanocomposite, the sensor offers a sensitivity of 64 mV/decade for nitrate detection, compared to 48 and 38 mV/decade for POT and MoS2 alone, respectively. The sensor was embedded into soil slurries where it accurately monitored nitrate for a duration of 27 days.

Keywords

Agricultural sensor, soil sensor, nitrate sensor, MoS2, fertilizer management

Disciplines

Agriculture | Electronic Devices and Semiconductor Manufacturing | Soil Science

Comments

This is a manuscript of an article publsihed as Ali, Md Azahar, Xinran Wang, Yuncong Chen, Yueyi Jiao, Navreet K. Mahal, Satyanarayana Moru, Michael J. Castellano, James C. Schnable, Patrick Schnable, and Liang Dong. "Continuous Monitoring of Soil Nitrate Using a Miniature Sensor with Poly (3-octyl-thiophene) and Molybdenum Disulfide Nanocomposite." *ACS Applied Materials & Interfaces* (2019). doi: 10.1021/acsami.9b07120. Posted with permission.

Authors

Md. Azahar Ali, Xinran Wang, Yuncong Chen, Yueyi Jiao, Navreet K. Mahal, Satyanarayana Moru, Michael J. Castellano, James C. Schnable, Patrick S. Schnable, and Liang Dong

Continuous Monitoring of Soil Nitrate Using a Miniature Sensor with Poly(3-octyl-thiophene) and Molybdenum Disulfide Nanocomposite

Md. Azahar Ali,[1,$] Xinran Wang,[1,$] Yuncong Chen,[1] Yueyi Jiao,[1] Navreet K. Mahal,[2] Satyanarayana Moru[1], Michael J. Castellano,[2] James C. Schnable,[3] Patrick S. Schnable,[2] and Liang Dong[1,*]

[1]Department of Electrical and Computer Engineering, Iowa State University, Ames, IA, USA-50011
[2]Department of Agronomy, Iowa State University, Ames, IA, USA-50011
[3]Department of Agronomy and Horticulture, University of Nebraska-Lincoln, Lincoln, NE, USA-68588

[$]Co-first authors (equal contribution to the work)

*Contact email: ldong@iastate.edu

KEYWORDS: Agricultural sensor, soil sensor, nitrate sensor, MoS_2, fertilizer management

ABSTRACT

There is an unmet need for improved fertilizer management in agriculture. Continuous monitoring of soil nitrate would address this need. This paper reports an all-solid-state miniature potentiometric soil sensor that works in direct contact with soils to monitor nitrate-nitrogen (NO_3^--N) in soil solution with parts-per-million (ppm) resolution. A working electrode is formed from a novel nanocomposite of poly(3-octyl-thiophene) and molybdenum disulfide (POT–MoS_2) coated on a patterned Au electrode and covered with a nitrate-selective membrane using a robotic dispenser. The POT–MoS_2 layer acts as an ion-to-electron transducing layer with high hydrophobicity and redox properties. The modification of the POT chain with MoS_2 increases both conductivity and anion exchange, while minimizing the formation of a thin water layer at the

interface between the Au electrode and the ion-selective membrane, which is notorious for solid-state potentiometric ion sensors. Therefore, the use of POT–MoS_2 results in an improved sensitivity and selectivity of the working electrode. The reference electrode comprises a screen-printed silver/silver chloride (Ag/AgCl) electrode covered by a protonated Nafion layer to prevent chloride (Cl^-) leaching in long-term measurements. This sensor was calibrated using both standard and extracted soil solutions, exhibiting a dynamic range that includes all concentrations relevant for agricultural applications (1–1500 ppm NO_3^--N). With the POT–MoS_2 nanocomposite, the sensor offers a sensitivity of 64 mV/decade for nitrate detection, compared to 48 and 38 mV/decade for POT and MoS_2 alone, respectively. The sensor was embedded into soil slurries where it accurately monitored nitrate for a duration of 27 days.

Introduction

Low-cost, high-performance nutrient sensors that continuously monitor soil conditions for precision agriculture,[1, 2] plant phenotyping,[3] and environmental quality[2] are in high demand. Soil is the primary source of nutrients for plant growth.[4-7] Biologically available soil nitrogen (N) is one of the key limiting factors in plant growth, and crop productivity relies heavily on the application of supplemental N in the form of fertilizer. Yet the proper amount of N fertilizer input can vary within fields by >100% per year due to variation in the soil N supply that is mostly caused by inter-annual weather variability. Insufficient N fertilizer input reduces crop production and excessive N input harms the environment. Farmer income suffers from both.

Continuous monitoring of N dynamics in agricultural fields would help maximize control over fertilizer management. Several laboratory-based soil N measurement methods are widely

used, such as gas chromatography-mass spectrometry (GC-MS), ultraviolet-visible (UV-VIS) spectrophotometry, ion chromatography (IC), chemiluminescence.[8-12] Although these methods are highly sensitive and selective and exhibit superior performance, they are known to have instrumentational complexity and need laborious and time-consuming tasks. Colorimetric determination of nitrate relies on reduction of nitrate by vanadium(III) combined with detection by the Griess reaction, and needs extraction of nitrate ions from soil samples using high-concentration (e.g., 2M) KCl solution, which limits its practical operation in fields.[7] With an increasing demand for on-site nitrate monitoring, mobile vehicle-based nitrate sensors[13] have been reported but still require significant labor and are relatively expensive. Satellite remote sensing[14] provides an indirect measure of plant N dynamics and does not currently provide high accuracy or spatial resolution. The development of field-deployable soil nitrate sensors is an attractive solution to better manage N fertilizer. Noteworthy in-field nitrate sensing methods include electrochemical sensors,[5,6,15] ion-selective electrodes (ISEs),[16,17] and microfluidic electrophoresis.[18] But, these miniature sensor methods need further development or remain challenging mainly due to the suboptimal sensitivity, relatively high signal drift, and material instability.[19]

Ion-selective membrane (ISM)-based sensors are considered a promising approach to detecting soil nutrients. Many ISEs are manufactured by simply coating thin metal wires with ISMs. However, redox-active charged species are difficult to transfer to metal wires, leading to a capacitive interface with the wire.[20] Conversely, non-metal wire-based ISEs often require an inner filling solution between the ISM and a conductive metal layer substrate;[21-25] their main drawbacks, however, include easy contamination of the filling solution with interfering ions, gradual

evaporation of the solution, variations in both osmolality and ionic strength, membrane delamination, poor adhesion, and difficulty in device miniaturization.[23,26]

Although ISEs that do not use inner filling solutions are an attractive option, a thin water layer that often forms at the interface between the conducting metal layer and the ISM has created a major challenge to the development of these sensors. Usually, this thin water layer presents an interfacial barrier to fast electron transfer and negatively impacts selectivity of the sensor to specific ions because different ions are trapped inside it.[27,28] Therefore, significant attempts have been made to replace the inner filling solutions with solid-contact materials as ion-to-electron transducing layers, with the objective of realizing an all-solid-state miniature ion sensor.[29-33] Many solid-contact candidate materials have been investigated, including hydrogel,[34] carbon nanotubes (CNTs),[35-36] graphene,[32] polymer-carbon composites,[37] metallic nanostructures,[38] macroporous carbon[39] and conjugated conducting polymers such as polyaniline,[19] poly(3,4-ethylenedioxythiophene) (PEDOT),[40] and poly(3-octylthiophene-2,5-diyl) (POT).[27, 41-42] Of these, PEDOT has a strong ability to oxidize to $PEDOT^+$, and thus has been extensively used as a solid-contact material[30] to attract lipophilic ions from the ISM to the conducting metal layer to establish potential equilibrium. As another promising candidate, electropolymerized[41-42] drop-casted,[43] and Langmuir–Blodgett[44] POT are redox sensitive, and can be oxidized reversibly in anion solutes with a low ohmic voltage drop; in addition, the high hydrophobicity of POT restricts the formation of a water layer between the POT and the ISM. Recently, the incorporation of 7,7,8,8-tetracyanoquinodimethane (TCNQ) into a POT matrix contributed to reducing the potential drift by more than one order of magnitude due to the introduction of a $TCNQ/TCNQ^-$ redox couple.[45] Despite its high redox property,[41] POT has a relatively low conductivity (approximately 10^-

^{6} S/cm)[28] and is also sensitive to light,[36] which negatively impacts the efficiency of charge transport through the POT to the conducting metal substrates.

Here, we report a miniature solid-state potentiometric sensor for the continuous monitoring of soil nitrate. The sensor uses a nanocomposite of POT and transition metal dichalcogenides of molybdenum disulfide (MoS_2) nanosheets[46] as a solid-contact ion-to-electron transducing layer. MoS_2 nanosheets provide large surface area, high conductivity,[47] insensitivity to light and pH, and absence of any side-reactions. The working electrode (WE) was built on top of a copper pad of printed circuit board (PCB) covered by a thin, patterned gold (Au) layer, a molybdenum disulfide (POT–MoS_2) nanocomposite-based solid-contact layer, and a nitrate-specific ISM. The incorporation of MoS_2 into POT not only increases the redox properties of POT,[48] but also maintains high hydrophobicity to minimize the formation of a thin water layer between the ISM and the Au layers. The use of POT–MoS_2 remedies the issue of the trapped water layer, thus contributing to increased charge transfer and ion selectivity of the WE.[49-51] The reference electrode (RE) of this nitrate sensor includes a silver/silver chloride (Ag/AgCl) electrode covered by a proton-exchange membrane to reduce redox reaction-induced chloride leaching from the RE, thus minimizing the drift of the reference potential. The sensor features an all-solid-state design that incorporates the POT–MoS_2 nanocomposite for improved device performance. The sensor can also be directly embedded in soil slurries for continuous measurement of nitrate dynamics for approximately four weeks. Furthermore, all the sensor materials (except for the screen-printed Ag/AgCl and evaporated Au) are deposited and patterned using a high-resolution dispensing robot with good control over the uniformity of material thickness.

Materials, Manufacturing, and Circuits

Materials: Methyltriphenylphosphonium bromide, polyvinyl chloride, Nafion, nitrocellulose, 2-nitrophenyl octyl ether, tetrahydrofuran, and tridodecylmethylammonium nitrate were purchased from Sigma Aldrich, MO. Polyvinyl butyral (PVB), regioregular POT, and Ag/AgCl ink (composed of finely dispersed chloritized silver flakes) were obtained from Fisher Scientific, MA. Ultrafine powders of MoS_2 nanosheets were obtained from Graphene Supermarket, NY. Deionized water with a resistivity of 18.2 MΩ cm was obtained using a purification system from Millipore, MA. Potassium nitrate (KNO_3), calcium sulfate ($CaSO_4$), sodium chloride (NaCl), sodium bicarbonate ($NaHCO_3$), and sodium phosphate monobasic (NaH_2PO_4) were also obtained from Fisher Scientific, MA. The PCB was manufactured by OHSPARK, OR.

The NO_3^- ISM cocktail contained methyltriphenylphosphonium bromide (0.25 wt. %), nitrocellulose (moistened with 2-propanol (35%); 1.93 wt. %), 2-nitrophenyl octyl ether (16.25 wt. %), polyvinyl chloride (5.75 wt. %), tetrahydrofuran (THF; 74.3 wt. %) and tridodecylmethylammonium nitrate (1.50 wt. %). This solution was sealed and stored at -20 °C.[52]

Nanocomposite of POT–MoS_2: The weight ratio of POT to MoS_2 was varied from 1:1 to 1:10 to study the influence of material composition on the redox properties of different POT–MoS_2 nanocomposites. In each case, the concentration of POT solution was fixed at 2.6 mg/mL. For example, in order to prepare a POT–MoS_2 sample with a 1:4 weight ratio of POT to MoS_2, 2.6 mg POT powders were dissolved in 1 mL THF solvent. 10.4 mg MoS_2 was added to the POT solution and sonicated for 4 h. Due to the attraction between the opposite charges of MoS_2 and POT, a homogeneous solution of POT–MoS_2 nanocomposite was formed.

Electronic Circuitry: A homemade data logger with embedded readout circuitry was used to detect and record potential variations between the WE and RE. The voltage potential provided by the sensor was first isolated from other parts of the readout circuit using two buffer amplifiers. Then, the output signal from the buffer amplifiers was fed to a differential amplifier to obtain a single output voltage, which could be further enhanced five-fold by using an inverting amplifier. Further, a voltage lifter circuit was introduced to obtain both negative and positive data from the sensor using a microcontroller. A two-order filter with 1 Hz cut-off frequency was then used to reduce the noise signal at the output. Finally, an Adafruit Feather 32u4 microcontroller was used to realize analog-to-digital signal conversion.

Device Fabrication: The sensor had two 5-mm-diameter, round-shaped electrodes formed on the PCB that served as the WE and RE. The rectangular pads on the PCB allowed for connecting the WE and RE to an external data logger. The base material of the WE and RE was copper. With the help of a shadow mask, a 5.2-mm-diameter and 100-nm-thick Au layer was deposited on top of one of the base electrodes using electron-beam evaporation. The same approach was used to form a 5.2-mm-diameter and 500-nm-thick Ag layer on top of the other base electrode. Figure 1 (a) shows a wafer-scale PCB containing arrays of RE and WE. To form the POT–MoS_2 nanocomposite and nitrate-selective ISM layers, a high-precision, automated fluid dispensing robot (Nordson EFD, RI) was used to dispense the prepared POT–MoS_2 and ISM solutions, respectively, on top of the Au surface (Fig. 1c). During this process, the POT–MoS_2 solution was first dispensed out of a syringe (size 10 cc) under an air pressure of 2 psi, followed by thermal treatment on a hotplate at 65 ºC for 1 h. After the ISM solution was dispensed, the WE was dried at room temperature for 10 h. The same material coating technique was applied to make other WEs using POT or MoS_2 alone as the solid-contact ion-to-electron transducing layer for comparison

with the proposed WE with the POT–MoS_2 nanocomposite. To form the RE of the sensor, the round-shaped Ag electrode was further screen-printed with Ag/AgCl paste using a stencil mask placed on top of the PCB. The 200-µm-thick Ag/AgCl paste was dried at 110 ºC for 2 h. To prevent the leaching of chloride ions as a result of the redox reaction of Ag/AgCl during long-term measurement,[53] a 15-nm-thick perfluorinated polymer layer, or Nafion was coated on the surface of Ag/AgCl using the above-mentioned fluid dispensing robot, and was then dried at 90 ºC for 1 h. In addition, the Nafion layer could also block anions entering the RE from the surrounding environment. Lastly, a 1.2-mm-thick waterproof insulating epoxy (Circuitworks, CW2500) was used to cover the PCB except for the regions of the WE, RE, and contact pads. This insulation layer impedes water penetration from the sidewalls of the coated materials when the sensor is embedded in soil slurries. The sensor was preconditioned by dipping it into 1500 ppm NO^-_3-N solution for 24 h. Figure 1c shows the fabricated solid-state nitrate sensor.

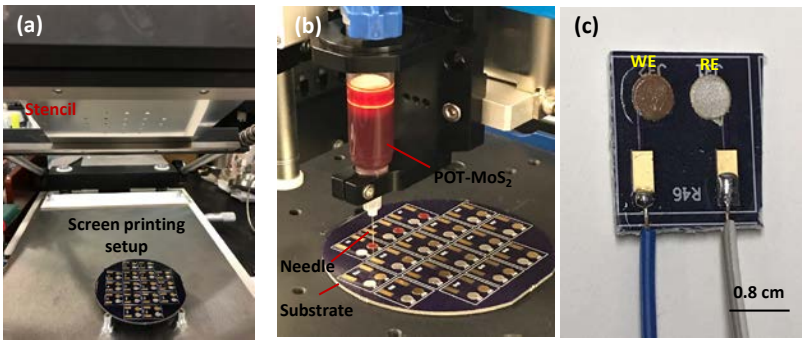

Figure 1. Step-wise representation of the fabrication of all-solid-state soil nitrate sensor. (a) Photograph taken during printing Ag/AgCl paste on circular-shaped silver (Ag) electrodes using a stencil printer. (b) Photograph taken during materials dispensing (POT–MoS_2 in THF solvent) on circular-shaped Au electrodes using a programmable high-precision. (c) Photograph of the device.

Working Principle

As the ion-to-electron transducing layer, the POT–MoS_2 nanocomposite layer undergoes a redox reaction during sensing. The mechanism of anion (or cation) exchanging through POT is demonstrated in the previously reported literature.[27] Si *et al.*, demonstrated a cyclic voltammetric experiment for anion (lipophilic) exchanging process in POT electrode-based ion selective membrane.[27] Kim *et al.*, also explained the anion-exchanging in POT film coated with ISM using ion-transfer stripping voltammetry.[42] Figure 2 shows the oxidation and reduction associated with the sensing mechanism. The mechanism for extracting electrochemically mediated anions (NO_3^-) into the ISM involves three phases,[27] including (1) oxidizing the POT–MoS_2 (or P) to $(POT–MoS)^+$ (or P^+); (2) triggering the extraction of NO_3^- from the test sample; (3) re-distributing lipophilic anions (R^-) from the ISM to the POT–MoS_2 layer. The corresponding redox reaction accompanied by NO_3^- transfer at the ISM is given by:

$$P^+_{(p)} + e^- + R^-(p) + NO_3^-{}_{(m)} \leftrightharpoons P_{(p)} + R^-_{(m)} + NO_3^-{}_{(aq)} \qquad \text{Eq. (1)}$$

where m, p, and aq represent the ISM phase, POT–MoS_2 nanocomposite phase, and aqueous phase, respectively, and $P_{(p)}$ and $P^+_{(p)}$ represent a few monomeric units of the POT chain in the neutral insulating state and the oxidized state with polaronic sites, respectively. Owing to the oxidation process (Fig. 2a), the POT–MoS_2 extracts the sample anions $NO_3^-{}_{(aq)}$ into the ISM and forces the redistribution of lipophilic anions (R^-) into the POT–MoS_2 layer. In the reduction process (Fig. 2b), the $(POT–MoS_2)^+$ becomes neutral POT–MoS_2, releasing the lipophilic anions R^- (p) into the ISM, which in turn leads to a release of $NO_3^-{}_{(aq)}$ from the outer membrane ($NO_3^-{}_{(m)}$) into the test solution. Therefore, by combining the redox and ion-exchange processes at the WE, an equilibrium is established at the aqueous-nanocomposite-ISM interfaces, leading to charge separation at each

interface, thus generating a phase-boundary potential.[12] This phase-boundary potential E_1 is given by $E_1 = \frac{RT}{zF} \times \ln a_I$, where, the R, T, z, F, and a_I represent the gas constant, temperature, charge of target ion, Faraday constant, and the primary ion activity without interfering ions. On the other hand, the RE of the sensor also undergoes a redox reaction, providing a constant potential (E_0).[54] The Nafion layer coated on the surface of the Ag/AgCl not only minimizes leaching of the chloride ion from Ag/AgCl, but also blocks other anions in the external environment from entering the RE. As the anions or cations move from high to low regions of concentration, a potential difference is produced during ion exchange. Therefore, the potential (E) is dependent on the logarithm of the ion activity and is described by the Nernst Equation:[55]

$$E = E_0 + E_1 = E_0 + \frac{RT}{zF} \ln a_I \qquad \text{Eq. (2)}$$

To determine the ion selectivity of the sensor, according to Nicolskii-Eisenman formalism,[56] the logarithm term in Eq. (2) can be replaced by a sum of selectivity-weighted activities given by:

$$E = E_0 + \frac{RT}{nF} \ln(a_I + K_{IJ}^{p} a_J^{Z_I/Z_J}) \qquad \text{Eq. (3)}$$

where K_{IJ}^{p} is the selectivity coefficient, a_I and a_J are the activities of I and J, respectively, in the test solution, and Z_I and Z_J are the charges of the primary and interfering ions, respectively.

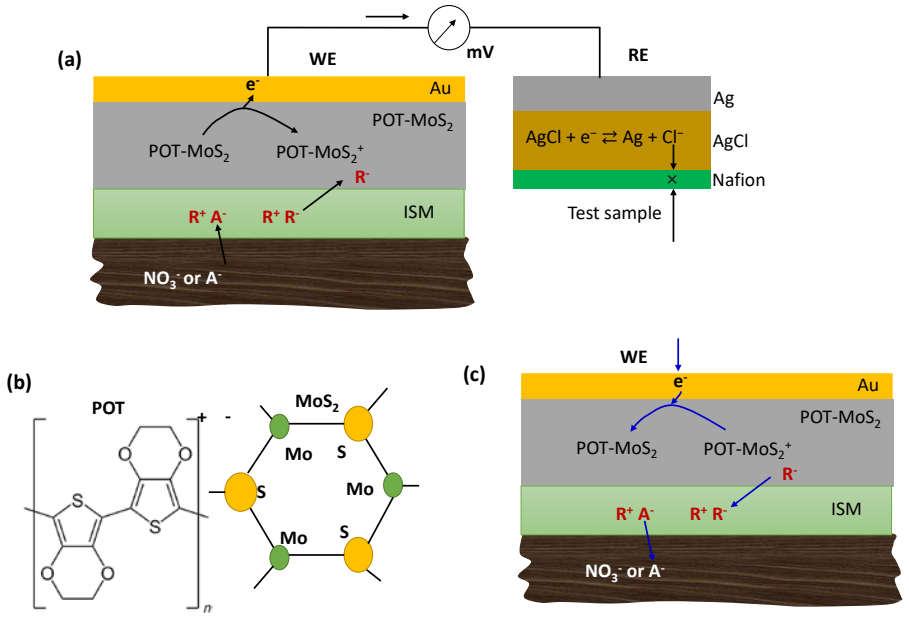

Figure 2. Schematic of the working principle of the soil sensor. (a) The oxidation process for the working electrode (ISM/POT–MoS_2/Au) in the presence of soil solution NO_3^- ions. R^+ and R^- represent anion and cation exchangers at the organic membrane, and M^+ and A^- are hydrophilic ions in soil water. POT–MoS_2 and POT–MoS_2^+ indicate neutral and oxidized POT–MoS_2 units. Oxidation/reduction is shown for the Ag/AgCl reference electrode. (b) Molecular structure of POT and MoS_2 for composite formation in this sensor. (c) Mechanism of the reduction process for the WE (ISM/POT–MoS_2/Au).

Results and Discussion

Surface Morphology and Water Repellent Properties: Figure 3 shows the scanning electron microscopic (SEM) images for different ion-to-electron transducing layers formed on the Au surface, including MoS_2, POT, and POT–MoS_2 nanocomposite. The MoS_2 layer is seen as a mixture of MoS_2 sheets of different sizes (Fig. 3a). The POT film exhibits continuous distribution and microtexture (Fig. 3b). In the POT–MoS_2 nanocomposite, MoS_2 sheets are embedded with POT due to the electrostatic interactions between them (Fig. 3c, d). In addition, Fig. 3e–g shows

the measured water contact angles of the MoS_2 (Θ = 68°), POT (Θ = 86°), and POT–MoS_2 (Θ = 107°) surfaces. With MoS_2, the nanocomposite remains hydrophobic, which may contribute to minimizing the formation of a thin water layer between the ISM and Au layers.

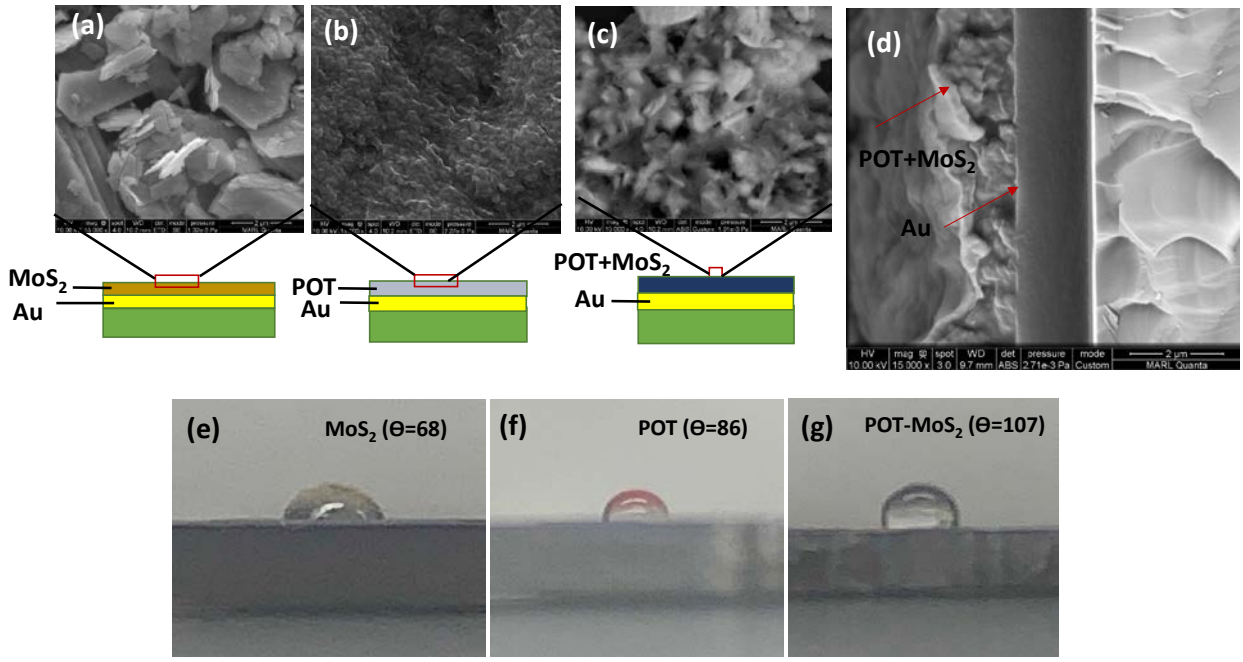

Figure 3. Scanning electron micrographs for MoS_2 sheets (a), POT (b), and POT–MoS_2 materials (c) with schematic representation of various layers. (d) Cross-sectional view of SEM image for POT–MoS_2 composite on Au. Contact angle (CA or Θ) studies for investigation of the hydrophobicity of the working electrode materials. A syringe was used to drop 3 µL volume of deionized water on the Au/PCB substrate coated with different working electrode materials, including MoS_2 (e), POT (f), and POT–MoS_2 (g). Images were analyzed using image J plugin software.

X-Ray Photoelectron Spectroscopic (XPS) Analysis: XPS measurement was conducted to confirm the chemical structures of MoS_2, POT–MoS_2, and ISM/POT–MoS_2. Figures 4a–c show the carbon 1s spectra of the MoS_2, POT–MoS_2, and ISM/POT–MoS_2 layers coated on the Au surface. After deconvolution into characteristic peaks, the C 1s peaks of MoS_2 are found at 284.9,

285.9, and 289.5 eV, indicating the presence of C–C, C–OH, and O–C=O groups, respectively.[57] The presence of carbon may be due to the impurity of the MoS_2 sheets. The incorporation of MoS_2 into the POT matrix leads to a shift in the peak location from 284.9 eV to 285.3 eV with a full-width half maximum of 2.5 eV (Fig. 4b), perhaps due to the POT hydrocarbons. A peak at 285.8 eV can be ascribed to the C–S bond, indicating the formation of strong chemical bonding at the interface between MoS_2 and POT. After the ISM was coated on the POT–MoS_2 layer, the peak for the C–C bond was found to be at 284.3 eV (Fig. 4c). Another peak at 286.1 eV was obtained on the surface of ISM due to the C–O group present in the ISM.

Figure 4d shows the MoS_2 layer with two S 2p core-level peaks of MoS_2 at the binding energies of 165.5 eV and 164.9 eV, corresponding to the S $2p_{1/2}$ and S $2p_{3/2}$ orbitals of divalent sulfide ions (S^{2-}). In Fig. 4e, two S 2p peaks appear at 162.7 eV and 163.9 eV due to the formation of S*–Mo and C–S*–C groups, respectively,[58] indicating incorporation of POT into MoS_2, and another peak found at 169.2 eV is associated with the S in sulfone. Furthermore, the S peaks were observed to shift towards higher energies of 1.6 eV and 1.2 eV due to the ISM coating on POT–MoS_2 film (Fig. 4f).

In the Mo 3d spectrum of MoS_2, a peak at 227.2 eV corresponds to S 2s with a chemical state of S^2, while other peaks at 229.9 eV, 233.1 eV, and 236.4 eV are ascribed to $Mo^{4+}3d_{5/2}$, Mo^{4+} $3d_{3/2}$, and Mo^{6+} $3d_{3/2}$, respectively (Fig. 4g). For the POT–MoS_2 (Fig. 4h), two additional peaks appear at 233.1 eV and 231 eV because of Mo^{6+} $3d_{5/2}$ and Mo^{5+} 3d, respectively. In the N 1s spectrum of ISM/POT–MoS_2 (Fig. 4i), the peaks seen at 402.7 eV and 408.4 eV correspond to -NH_2 and nitrooxy (-N-NO_2) groups due to the presence of nitrocellulose in the ISM. Therefore, the formation of a composite between POT and MoS_2 due to the appearance of chemical C-S bond is

confirmed. Further, the presence of -NH_2 and nitrooxy (-N-NO_2) groups at ISM/POT–MoS_2 indicates the ISM coating on the surface of the POT–MoS_2 matrix.

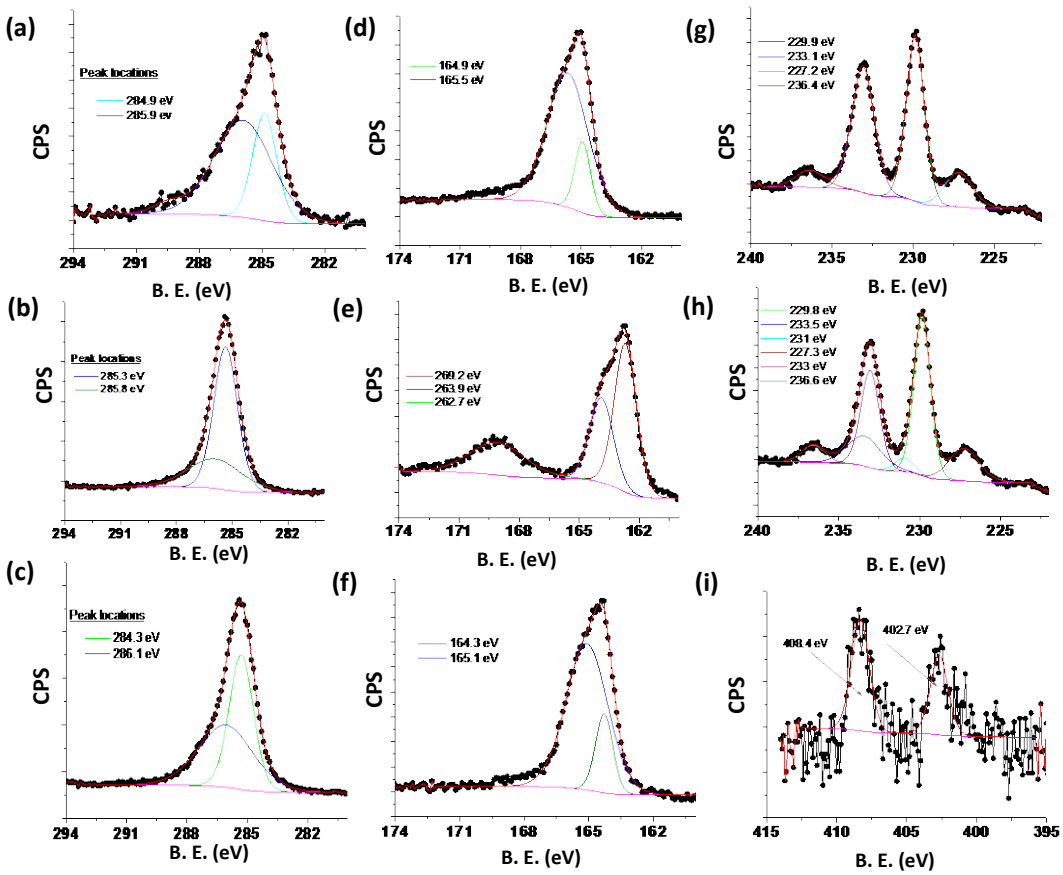

Figure 4. XPS analysis for the working electrodes using MoS_2, POT–MoS_2, and ISM/POT–MoS_2 materials. XPS spectra of the carbon 1s region of MoS_2 (a), POT–MoS_2 (b), and ISM/POT–MoS_2 (c). Sulphur (S 2p) peaks for the MoS_2 (d), POT–MoS_2 (e) and ISM/POT–MoS_2 (f) electrodes. XPS peaks for molybdenum (Mo) 3d found for the MoS_2 (g) film and POT–MoS_2 (h) film. XPS spectra for the nitrogen 1s peaks region of ISM/POT–MoS_2 film.

Electrochemical Characterizations: Cyclic voltammetry (CV) was conducted at room temperate to investigate the redox properties of the MoS_2, POT, POT–MoS_2, and ISM/POT–MoS_2 layers coated on the Au electrodes (Fig. 5a), and the POT to MoS_2 ratio of the composite was set

to 1:4. The cyclic voltammograms for the MoS_2-, POT-, and POT–MoS_2-based electrodes exhibited clear reversible oxidation and reduction reactions for the $[Fe(CN)_6]^{3-/4-}$ redox probes. The oxidation current for the POT–MoS_2-based electrode was higher (115 µA) than that for the MoS_2-based electrode (90 µA) and that for the POT-based electrode (65 µA), because the incorporation of high-conductivity MoS_2 facilitates an improved electron transfer from the POT–MoS_2 to the Au current conductor. Also, the values of peak-to-peak potential difference (ΔE) for the POT- and POT–MoS_2-based electrodes were found to be 0.127 V and 0.38 V, respectively. After modification with the ISM, the POT–MoS_2-based electrode exhibited reduced oxidation and reduction peaks for the $[Fe(CN)_6]^{3-/4-}$ redox probes, perhaps due to sluggish ion exchanges, or a high selectivity of ISM that rejected $[Fe(CN)_6]^{3-/4-}$ ions (inset of Fig. 5a).

To optimize the weight ratio of POT to MoS_2 in composite formation, CV measurements were taken for composites at varying weight ratios with the objective of obtaining the composite that offered the largest value of ΔE. Figure 5b shows that as the weight ratio of POT to MoS_2 changes from 1:1 to 1:10, the obtained ΔE increases at lower weight ratios, reaches a maximum ΔE = 0.345 V at a 1:4 weight ratio, and then deceases at higher weight ratios. Further, Fig. 5c shows that the oxidation current decreases with increasing POT–to-MoS_2 weight ratios from 1:1 to 1:3, due to a reduction in the free POT in the POT–MoS_2 matrix. At a weight ratio between 1:4 and 1:6, the oxidation current is observed to be relatively stable at a low value, due to the full bond formation. With further increase in the MoS_2 component, the free MoS_2 in the matrix prompts the oxidation current due to the inherent electroactivity of MoS_2 (Fig. 5c). Therefore, for the potentiometric measurement, the optimum POT-to-MoS_2 weight ratio was chosen to be 1:4.

Figure 5d presents the redox activity studies of the POT–MoS_2 based electrode (POT-to-MoS_2 weight ratio: 1:4). The POT-MoS_2 based electrode shows well-redox behavior for the oxidation

and reduction of ferro/ferricyanide redox species. The difference between the oxidation and reduction potentials is found to increase with an increase in scan rate. The peak current is proportional to the square root of the scan rate (inset of Fig. 5d), indicating a diffusion-controlled process on this redox sensitive material.

For open circuit potential (OCP) measurement, the MoS_2, POT, and POT–MoS_2 layers were coated with nitrate-specific ISM. Figure 5e shows the output voltage signals of the fabricated sensors in response to 1000 ppm NO_3^--N. The magnitude of the potential for the POT–MoS_2-based electrode exhibits a maximum value of 325 mV, higher than the counterpart electrodes using POT (255 mV) and MoS_2 (66 mV). As is evident in the CV studies (Fig. 5a), compared to the POT alone, the POT–MoS_2 nanocomposite offers a better redox property, such as good electro-active mediator to allow selective interaction with NO_3^- ions in the surrounding solutions, (Fig. 3a–b), thus providing an increased OCP.

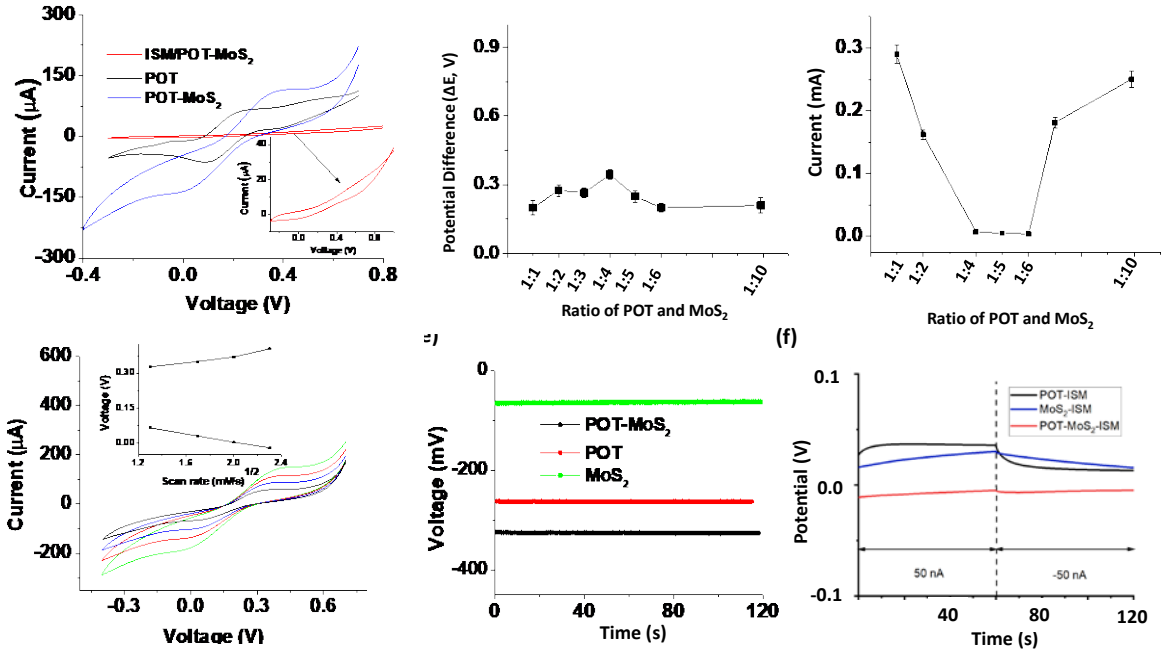

Figure 5. (a) Cyclic voltammogram (CV) for different electrodes (a) MoS_2, POT, POT–MoS_2 and ISM/POT–MoS_2. These experiments were conducted using phosphate-buffered saline (PBS)

solution mixed with a ferro/ferricyanide ($[Fe(CN)_6]^{3-/4-}$) of concentration 2 mM. Inset shows zoom CV curve of ISM/POT–MoS_2. (b) Potential differences (ΔE) obtained from CV curves were plotted against the ratio of POT–MoS_2-based electrodes. In the composite formation, the ratio of POT-to-MoS_2 was varied from 1:1 to 1:10 by weight percentage. (c) Oxidation current obtained from CV curves vs. ratio of POT to MOS_2 (1:1 to 1:10), and (d) CV graphs for the optimized electrode based on POT–MoS_2 (at ratio 1:4) in the presence of $[Fe(CN)_6]^{3-/4-}$. (e) Voltage measurements (open circuit potential) for three electrodes, such as MoS_2-, POT-, and POT–MoS_2-based sensors, after coating with nitrate-ion selective membrane in the presence of 1000 ppm NO_3^--N. (f) Chronopotentiometry measurements for three nitrate sensors using POT, MoS_2 and POT-MoS_2 as ion-to-electron transducing layers. Constant 50 nA anodic and cathodic currents were applied uninterruptedly for 60 s each and the respective potential responses over time were recorded.

The potential stability of the electrodes and the electrical capacitance of the solid contact were evaluated using chronopotentiometry[19] (Figure 6f). The characteristic chronopotentiometric curves present the change in potential over time measured in a 500 ppm NO_3^--N solution. The obtained results are shown in Fig. 6. The potential drift of electrode was calculated as $\Delta E/\Delta t$. The $\Delta E/\Delta t$ values for the POT, MoS_2 and POT-MoS_2 based nitrate-selective electrodes were found to be 115.4 μVs^{-1}, 213.3 μVs^{-1}, and 95 μVs^{-1}, respectively. Similarly, the low-frequency capacitances C of the POT, MoS_2, and POT-MoS_2 based electrodes were estimated to be 433 µF, 234 µF, and 526 µF, respectively, according to the equation $\Delta E/\Delta t = I/C$. These results indicate that the POT-MoS_2 based electrode has a larger capacitance and a lower potential drift compared to the electrode using POT or MoS_2 (see Table S1, Supporting Information).

Quantification of Nitrate-Nitrogen

Nitrate detection by the sensors using MoS_2, POT, and POT–MoS_2 as the solid-contact ion-to-electron transfer layer materials was investigated. Figure 6a shows the calibration curves, i.e., the OCP values of the sensors as a function of nitrate concentration ranging from 1 to 1500 ppm (NO_3^-

-N). The slope of the voltage response versus logarithm concentration for the POT–MoS_2-based sensor is 64 mV/decade (10-1500 ppm), which is higher than the POT (approximately 48 mV/decade, 10-1500 ppm) and the MoS_2 (approximately 38 mV/decade, 10-1500 ppm). The high electro-activity and redox property of the POT–MoS_2 layer is believed to contribute to improved sensitivity in nitrate detection. In addition, the high hydrophobicity of the POT–MoS_2 layer could minimize water accumulation between the ISM and the Au current collector, lowering the barrier of charge transfer to the Au layer and thus improving the sensor sensitivity. Although the MoS_2-based sensor also provides a wide dynamic range up to 1000 ppm (NO_3^--N); the output voltage was found to be unstable (particularly during the detection of high nitrate concentrations), possibly due to poor adhesion of the MoS_2 layer to the ISM layer, leading to membrane delamination. Following the method described in Buck *et al.*,[59] we calculated the limit of detection (LOD) as 0.84 ppm, 1.3 ppm and 1.4 ppm for the three sensors using MoS_2, POT and POT-MoS_2, respectively, according to the obtained calibration plots in Fig. 6a. Table 1 compares nitrate monitoring using different nanostructured materials. The laboratory-based nitrate measurement methods based on Griess assay, UV-VIS spectrophotometry, GC-MS and chemiluminescence for nitrate monitoring in different medium showed higher performance in terms of their limit of detection compared to the POT-MoS_2 based sensor. However, our sensor can conduct long-term measurements, exhibit a wider detection range, and have considerable performances suitable for field applications.[8-12] In addition, our sensor uses an integrated solid-state RE, thus offering the possibility of miniaturization and mass production, while the above-mentioned counterpart sensors require commercial large-sized REs. The sensor is used in direct and long-term contact with soil particles across a range of wetness for nitrate quantification.

Table 1. Comparison for NO_3^--N monitoring using different nanomaterials and techniques.

Electrode materials or Transducers	Methods	Test range (ppm)	Detection limit (ppm)	Sensitivity (mV/dec)	Test period and environment	Ref.
CNTs	OCP	0.14×10^{-3}-14.02	0.0014	58.9	NA	60
Polypyrrole	OCP	0.14-1400.6	0.42	53.9	7 d in water	61
Graphene	OCP	0.14-1400.6	0.3	54.8 ± 2.5	Not tested	62
Polypyrrole	OCP	1.4-56.1	1.68	51.6	Not tested	63
POT	OCP	0.14-1400.6	NA	53	~90 d in water	64
Poly(aniline)	OCP	0.14-1400.6	NA	51.5	~90 d in water	64
PEDOT	OCP	0.011-63.34	0.25	NA	NA	65
Ionic liquid	OCP	0.044- 442.8	0.012	60.1	NA	66
Graphene–tetrathiafulvalene	OCP	0.004-442.8	~0.004	59.14	NA	67
Carbon black	OCP	0.044- 442.8	0.1	60	NA	68
Tetrathiafulvalene	OCP	0.044- 442.8	0.01	58.8	NA	69
Spectroscopic	VCl_3/Griess	0.02–5	0.016	NA	NA	8
Optical	Greiss	0–9.3	0.027	NA	Sea water	9
Optical	UV	0.3-3.1	0.007	NA	Waste water	10
Optical	Chemiluminescence	0.001-0.9	0.001	NA	Atmospheric	11
Gas chromatography	Nitration	0.062-6.2	0.1	NA	~3d in	12
POT–MoS_2	OCP	1-1500	1.3	64	25 d in soil	This work

Selectivity, Repeatability, and Stability Studies: Figure 6b shows the selectivity of the sensors using the MoS_2, POT, and POT–MoS_2 as the ion-to-electron transducing layers in the presence of interfering anions such as chloride (Cl^-), phosphate (PO_4^{3-}), bicarbonate (HCO_3^-), sulfate (SO_4^{2-})

and nitrite (NO_2^-). The selectivity coefficient, K_{IJ}^p, described in Eq. 4, is a numerical measure of how adequately the sensor is able to discriminate against the interfering ions.

$$K_{IJ}^p = \frac{a_I}{a_J^{z_I/z_J}} \qquad \text{Eq. 4}$$

where a_I, a_J, Z_I, and Z_J are the activity of primary ions, activity of interfering ions, charge of the primary ions, and charge of the interfering ions, respectively. According to IUPAC recommendations, a matched potential method, including the separate solution method (SSM), is practical and unique for estimating K_{IJ}^p , which does not depend on the Nicolskii–Eisenman equation.[70-71] In the SSM method, the potential of the sensor is adjusted by introducing two different concentration solutions separately, wherein one contains the ion I with activity a_I (no J), and the other one contains the ion J with the same activity a_J (no I) to attain the same measured potential. To calculate the value of K_{IJ}^p, the a_I was calculated from the extrapolated calibration graph where the potential of the interfering ion concentration (a_J) is equal. The result demonstrates that the POT–MoS_2 based sensor shows less susceptibility to PO_4^{3-} and SO_4^{2-} than the sensor using POT or MoS_2 alone as the transducing layer, perhaps due to the improved hydrophobicity of the POT–MoS_2 layer, while the influence of HCO_3^- and Cl^- on the output potential is comparable between all the sensors. For NO_2^-, the sensors based on POT or MoS_2 showed more negative selectivity coefficients compared to the POT-MoS_2 based sensor.

Figure 6c shows the stability of fabricated Nafion-modified Ag/AgCl RE with respect to commercial RE by varying the KCl concentration from 0.01 M to 3 M KCl. Without the Nafion coating, the Ag/AgCl electrode shows a stable OCP with 0.01 M and 0.05 M of KCl concentration, however, with a higher concentration of KCl, such as 1 and 3 M, the electrode shows a significant potential change. This change of potential is due to the considerable electrochemical reaction in

the AgCl layer, which may leach Cl^- ions from the AgCl layer, resulting in unstable OCP. With increasing KCl concentration, the Nafion-modified Ag/AgCl electrode does not show a change in the OCP. The pronated Nafion layer on the Ag/AgCl surface acts as a protective layer that does not allow Cl^- ions to leach out and rejects Cl^- from outside the Nafion. Figure 6d shows the long-term stability (approximately 32 d) of the fabricated solid-state Ag/AgCl electrode with and without a Nafion layer in the presence of 0.01 M of KCl. With no Nafion coating on the Ag/AgCl surface, the OCP was not constant in long-term measurements due to Cl^- leaching. However, blocking the Ag/AgCl surface with Nafion resulted in an almost constant OCP for 32 d with minimum drift. This indicates that Nafion-coated Ag/AgCl is not externally influenced by Cl^- ions and is more stable for long-term measurement.

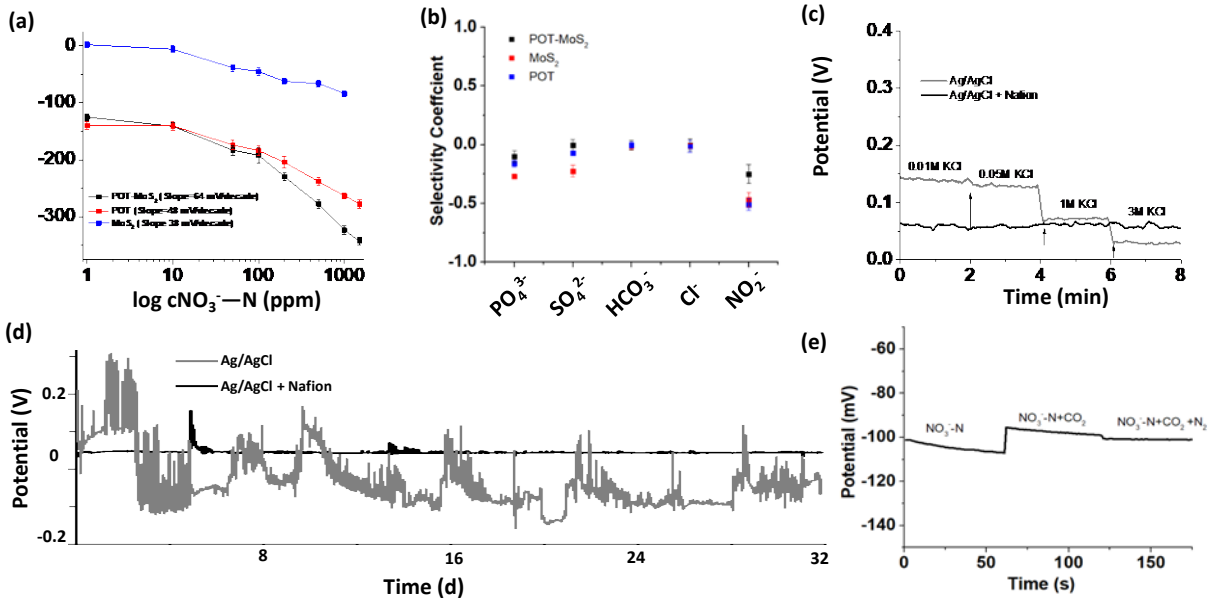

Figure 6. (a) Sensor responses in millivolts (mV) made by MoS_2, POT, and POT–MoS_2 electrodes modified with ISM. A stock solution of 1500 ppm of nitrate-nitrogen was made in DI water and diluted from 1500 ppm to 1 ppm. Sensor measurements were conducted for 2 min at each concentration. Corresponding average voltages for all the sensors (MoS_2, POT, and POT–MoS_2) were plotted against the logarithm of nitrate-nitrogen in ppm. Error bars were calculated using three consecutive measurements for each concentration. (b) For the selectivity studies, the NO_3^--N concentration was set to 100 ppm, and the hydrophilic interfering ions were set to 400 ppm. The

selectivity coefficients were calculated for MoS_2, POT, and POT–MOS_2-based ISM sensors using the separate solution method (SSM). (c) The stability of the fabricated RE (Ag/AgCl) with and without Nafion coating was tested separately by varying the concentration of KCl from 0.01 M to 3 M. For the stability test, the OCP of the fabricated RE was measured with respect to a leak-less miniature Ag/AgCl RE having an internal electrolyte of 3.4 M KCl (obtained from EDAQ, ET072-1). (d) Long-term stability measurement of the Ag/AgCl electrodes with and without Nafion coating: plot of the OCP of the electrodes vs. time in the presence of 0.01 M KCl solution. (e) Interference studies of the POT-MoS_2 based sensor in presence of CO_2 and N_2 gases purging into a nitrate solution. After the nitrate measurement, the sensor was tested in a closed chamber where CO_2 and N_2 gases continuously flowed for 15 minutes before the measurement.

To investigate the repeatability of the sensor, we repeatedly measured the OCP as the sensor was transferred between 1 ppm and 1300 ppm NO_3^--N (Fig. S3, Supporting Information). For 12 repeated measurements, the sensor was dipped with high nitrate-nitrogen (1300 ppm) for 2 min, and the OCP was recorded. Then, the sensor was immediately dipped in low concentration nitrate-nitrogen (1 ppm), and then washed with DI water for another 2 min, and the OCP was recorded. The sensor responded within less than 5s when switching from high to low concentration, or vice versa. With a high concentration of NO_3^--N (1300 ppm), the percentage of relative standard deviation for the output voltage was calculated as ±3.0%, while with a low concentration, the sensor showed a deviation of ±5.0 % over six repeated measurements. This result indicates high repeatability of the test.

For the interference study in presence of CO_2, the POT-MoS_2 based sensor was tested in a closed chamber with a controlled CO_2 environment (Figure 6e). Before the measurement the CO_2 gas (saturated) was injected into a nitrate solution for 15 minutes to ensure satirized dissolved CO_2 in the solution. The test result shows that the introduction of CO_2 into the solution led to a ±5% relative deviation from the initial signal of the sensor. This may be caused by a pH change induced by the dissolved CO_2 in the solution. Also, we found that the introduction of N_2 into the solution

had almost no influence on the sensor readout. Nevertheless, the sensor exhibited a good potential stability in the CO_2 environment.

We studied reproducibility of the POT-MoS_2 based nitrate electrode (Figure S1, Supporting Information). The concentration of NO_3^--N was set to 100 ppm in DI water and the measurement was performed for 2 min for each POT-MoS_2 electrode. The results show that the variation in potential among these electrodes is negligibly small, as evident by its low relative standard deviation (RSD = ~3.5%) due to the uniform coating of the electrode materials (i.e., POT-MoS_2 ad ISM) using a high-resolution robotic dispensing machine.

We carried out potential stability measurement for the POT-MoS_2 based nitrate sensor over ~10 days (Figure S2, Supporting Information). The electrode was pre-conditioned in a 1500 ppm NO_3^--N solution for 3 days. The result of the continuous measurement shows the potential at day 10 (~ -184 mV) remained almost unchanged from the initial potential (~-186 mV). Therefore, the pre-conditioned electrode was found relatively stable.

Nitrate Measurement in Extracted Soil Solution: To demonstrate nitrate measurement in extracted soil water, soil water was extracted from three locations at the Iowa State BioCentury Research Farm (Ames, IA) using a suction lysimeter. The suction head of the lysimeter was inserted at a depth of 25 cm from the soil surface. As the POT–MoS_2 based sensor was dipped into different test solutions, the sensor responded by providing different voltage signals (Fig. 7a). The inset of Fig. 7a shows the converted nitrate concentration using the calibration curve of the sensor (Fig. 6a). For comparison, a commercial sensor (LAQUA HORIBA nitrate sensor) was used to measure the same sample solutions. Our sensor and the commercial sensor showed comparable readings.

Short-Term Nitrate Measurement in Soil Column: To demonstrate short-term nitrate measurement in a soil column, two identical POT–MoS_2 based sensors were fixed on the walls of two column beakers filled with soil slurries (Fig. 7c). The column beakers were 6 cm in diameter and 10 cm in height and loaded with soils to a height of 9 cm from the bottom of the beaker. Several 3-mm-diameter holes were created at the bottom of beaker to flush out the water. Each sensor was located 7 cm from the bottom, as shown in Fig. 7b. The soil used here was collected from the soil surface at the research farm mentioned above. During the demonstration, the soil in one beaker was flushed with alternating solutions of 0 and 50 ppm NO_3^--N at different time points, each time lasting 2 min, while the soil in the other beaker was flushed with 0 and 100 ppm NO_3^--N. Figure 7d shows the voltage outputs of the two sensors installed in the two beakers. When the soil was flushed with DI water (0 ppm), the output voltage of the sensor reached a baseline voltage of approximately -110 mV. When the soil was treated with 50 ppm or 100 ppm nitrate solution, the sensor 1 and sensor 2 outputs went down to approximately -123 mV or approximately -150 mV, respectively. Figure 7e shows the nitrate concentrations converted from the voltage outputs of the sensors. It should be noted that the converted concentrations are evidently lower than the known input nitrate concentrations. The nitrate solution was flushed out of the soil slurries immediately after introducing the solution, and the pre-wetted soil particles already had water content that may have diluted the external original concentration of nitrate in the testing soil slurries, resulting in reduced ppm levels compared with the original input concentration of nitrate. Alternatively, when we introduced the external nitrate concentration into the soil, as nitrate has a low charge density compared to other common pre-existing anions in soil solution and they always occupy the few positively charges sites, in turn, the nitrate ions may have failed to bind with soil particles within a short period of time or denitrification of nitrate ions, thus both sensors showed

reduced ppm nitrate levels. However, the sensor response returned to the baseline ppm level immediately as we flushed with DI water.

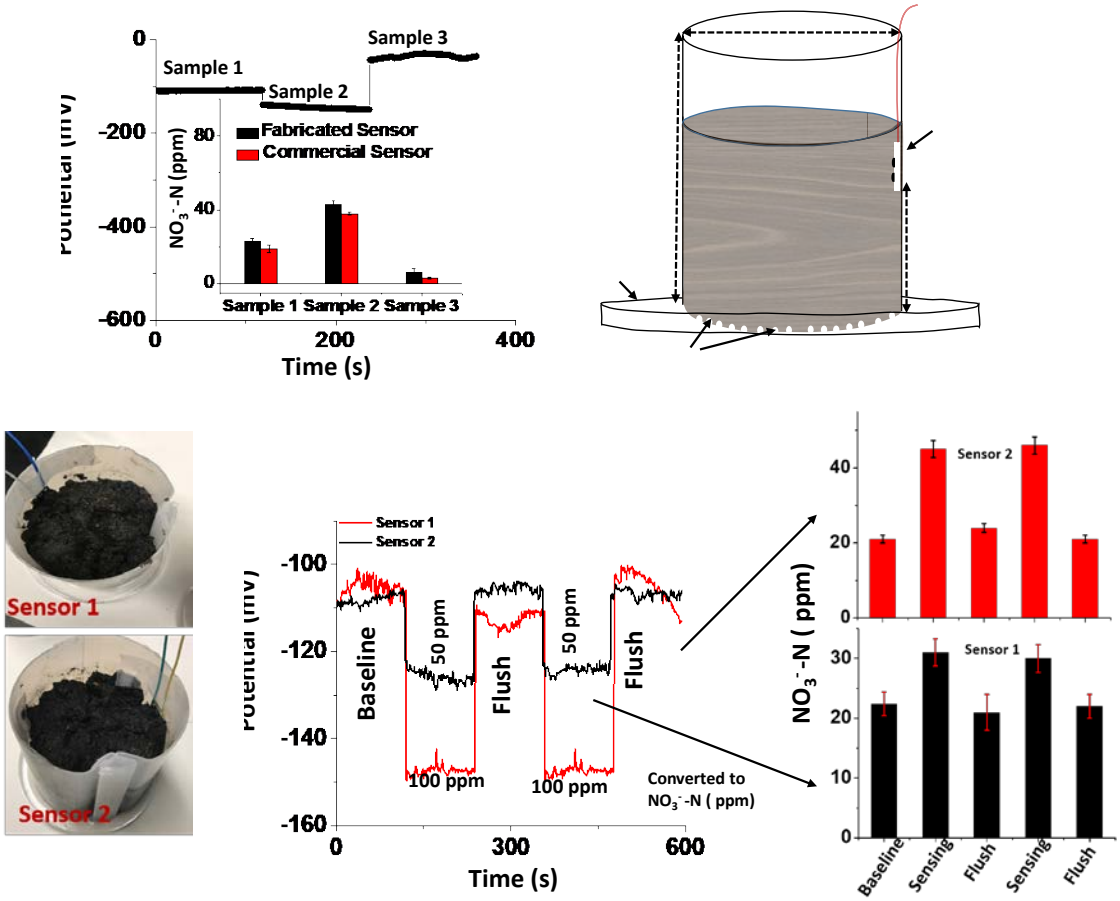

Figure 7. (a) Sensor responses (commercial and fabricated) for real soil extracted solutions collected directly from Ames, Iowa with a suction lysimeter. (b) Schematic presentation of soil-column setup for nitrate-nitrogen measurement. (c) Photographs of soil-column beakers with soil slurries wherein the sensors were hung on the wall of the column. (d) Short-term soil nitrate-nitrogen sensing in the soil column, where the baseline was set in the presence of DI water (baseline), and the column was flushed with DI water after the soil was treated with 100 and 50 ppm of NO_3^--N, and (e) Plot for corresponding sensor readings.

For long-term measurement, two identical sensors (sensor 1 and sensor 2) were deployed directly into soil slurries in column beakers over approximately 4 weeks with different rates of nitrate concentration (50 and 100 ppm NO_3^--N), and OCP was measured continuously (Fig. 8a–b). For this measurement, the beaker dimensions were the same, and the sensors were fixed at the same location as for the short-term measurement. However, unlike the previous design of the beakers for short-term measurement, there were no holes at the bottom of the beakers to promote denitrification of nitrate ions in the soil slurries before evaporation.

The long-term monitoring of nitrate in soil slurries using sensor 1 and sensor 2 is shown in Fig. 8c and Fig. 8d–e, respectively. For sensor 1, when the soil beaker was treated with DI water, the NO_3^--N level was found to be approximately 14–23 ppm (Fig. 8c, marked with box) which is a similar result to that observed in the short-term measurement. Due to the slow diffusion of pre-occurring nitrate ions from the soil slurry into the water, the nitrate level slowly increased after water was poured until it reached a maximum concentration. Further, the sensor showed a slow decrease in NO_3^--N concentration to the range of 2–5 ppm due to denitrification at room temperature (25 ºC). In this parched soil condition, the nitrate ppm was found to be almost constant. Upon further repeating the experiment two times, the sensor showed similar results.

Interestingly, when the 50 ppm of NO_3^--N was poured into the soil beaker, sensor 1 began to show a slow increase in NO_3^--N, and reached a maximum value of 53 ppm NO_3^--N. With the addition of external nitrate into the soil, the sensor took approximately 3 hours to reach a maximum nitrate level, indicating slow diffusion of nitrate ions into the soil. This is because when soil particles at the sensor interface are completely wet, nitrate ions may diffuse slowly from the external nitrate solution (as we filled the beaker) due to the concentration gradient. The NO_3^--N concentration was further decreased to a low value of 2–5 ppm when the soil particles became

parched due to water evaporation, which restricted the mobility of the nitrate ions. Sensor 1 showed an almost similar performance of NO_3^--N, while the sensor was further flushed with 50 ppm NO_3^--N concentration another three times. When more water containing NO_3^--N (see the last two repeated measurements, Fig. 8c) was poured, the sensor showed a longer nitrate response at 50 ppm, as the evaporation of water from the soil takes time.

Similarly, for sensor 2, the sensor performance was investigated in the presence of DI water and 100 ppm of NO_3^--N concentration for 2 weeks (Fig. 8d), and the sensor was kept in parched soil conditions for another 2 weeks (Fig. 8e). With DI water filling, the sensor exhibited a concentration of approximately 20–25 ppm of NO_3^--N due to the pre-existing nitrate ions in the soil. Further, the soil water content dried slowly, and the soil became parched under this condition. The sensor showed a similar NO_3^--N response as was observed in the case of sensor 1. When the soil slurry was flushed with 100 ppm NO_3^--N solution, the output of the sensor reached a maximum value of NO_3^--N (approximately 104 ppm), after which the sensor response began to decay to less than 10 ppm of NO_3^--N due to water evaporation. Further, sensor 2 was kept in the same soil without the addition of water for approximately 2 weeks, and the concentration variability was investigated (Fig. 8e). The soil become parched without the addition of water and NO_3^--N solution. Under this condition, however, the sensor still exhibited a low ppm of nitrate (approximately 10–2 ppm). Interestingly, the sensor response decreased from approximately 10 ppm to 3 ppm over a long period of time (13 d), but the sensor response was found to be irregular, perhaps because of the changing room temperature or humidity level. The sensor deployed into soil slurries can monitor nitrate-nitrogen accurately monitored for at least a duration of 27 days.

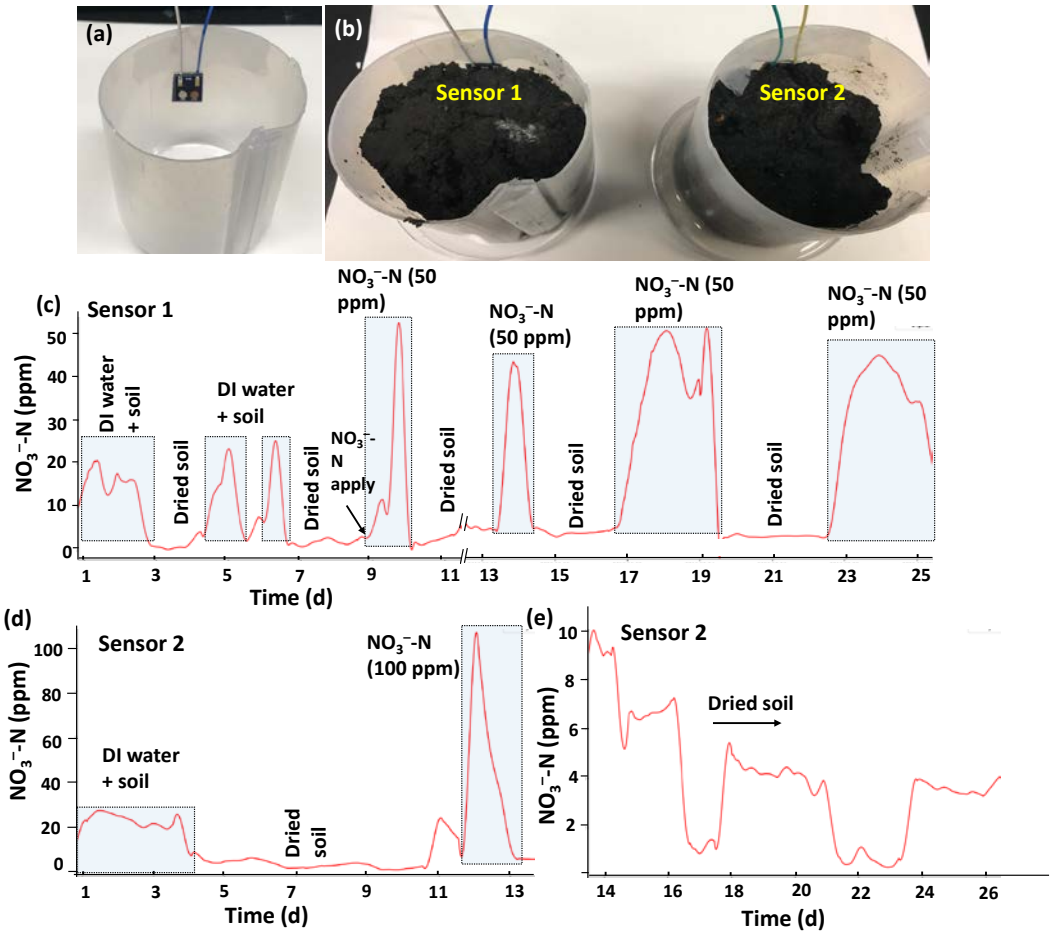

Figure 8. Long-term measurement (approximately 4 weeks) using two different individual sensors (made with POT–MoS_2 material), wherein sensor 1 and sensor 2 were deployed in beakers containing soil slurries. Photographs of column beakers without soil slurries (a), and with soil slurries and sensor 1 and sensor 2 (b). For sensor 1 (c), the soil beaker was filled with DI water and then left to dry, and the soil slurry was again treated with water multiple times and then parched. Finally, DI water mixed with nitrate-nitrogen (50 ppm) was poured into the soil slurry in the column beaker with sensor 1 and left to dry. The process was repeated multiple times (for approximately 4 weeks) for sensor 1. For sensor 2, the soil slurry was initially filled with DI water, parched, and flushed with 100 ppm nitrate-nitrogen (d). After drying, sensor 2 was kept in the parched condition for about 2 weeks (e).

Conclusion

In this manuscript, a novel all-solid-state miniature sensor designed for long-term use in continuous monitoring of soil nitrate was presented. The sensor was fabricated on a PCB using patterned WE and RE. To characterize the sensor materials, solid-state components using MoS_2, POT, and POT–MoS_2 were directly coated on the patterned PCB and functionalized with an ISM using a high precision robotic-armed auto-dispenser machine. The electro-activity properties of POT–MoS_2 composite were found to be excellent, and the material was used as an ion-to-electron transducing layer for nitrate detection in the sensor. The POT–MoS_2 composite material produced superior sensor performance in terms of selectivity and sensitivity compared with MoS_2 and POT, and the reported nitrate sensors shown in Table 1. This may be the result of the high hydrophobicity and high redox properties of the POT–MoS_2 layer. The solid-state sensor is selective to nitrate ions even when other anions are present at significant concentrations and offers long-term stability. This sensor can be deployed into the soil for long-term nitrate monitoring (about 4 weeks). In the future, by replacing the ion selective membrane, the sensor could be adapted to detect other soil nutrients, including potassium, phosphate, and sulfate. These other nutrients are also essential to plant growth and agricultural productivity. Continuous measurement of these nutrients thus have significant potential applications in plant biology, plant breeding, environmental science, and production agriculture.

Supporting Information

Reproducibility, repeatability studies and potential stability of the sensor. This material is available free of charge via the Internet at http://pubs.acs.org.

Conflict of interest:

EnGeniousAg LLC (Ames, Iowa) has a license from Iowa State University Research Foundation to use this technology.

AUTHOR INFORMATION

Corresponding Author

*Liang Dong; E-mail: ldong@iastate.edu; Phone: +1-515-294-0388.

Acknowledgement

The information, data, or work presented herein was funded in part by the Advanced Research Projects Agency-Energy (ARPA-E), U.S. Department of Energy, under Award Number DE-AR0000824. The views and opinions of authors expressed herein do not necessarily state or reflect those of the United States Government or any agency thereof. This project was also partially supported by the United State Department of Agriculture (USDA) under the grant number 2017-67013-26463, the National Science Foundation (NSF) under the grant number IOS-1650182, and the Plant Sciences Institute at Iowa State University.

References

1. Lipper, L.; Thornton. P.; Campbell, B. M.; Baedeker, T.; Braimoh, A.; Bwalya, M.; Caron, P.; Cattaneo, A.; Garrity, D.; Henry, K.; Hottle, R. Climate-Smart Agriculture for Food Security. *Nat Clim Chang.* **2014,** *4*, 1068.
2. Walter, A.; Finger, R.; Huber, R.; Buchmann, N. Opinion: Smart Farming is Key to Developing Sustainable Agriculture. *Proc. Natl. Acad. Sci.* **2017,** *114*, 6148-50.

3. White, J. W.; Andrade-Sanchez, P.; Gore, M. A.; Bronson, K. F.; Coffelt, T. A.; Conley, M. M.; Feldmann, K. A.; French, A. N.; Heun, J. T.; Hunsaker, D. J.; Jenks, M. A. Field-based Phenomics for Plant Genetics Research. *Field Crop. Res.* **2012,** *133*, 101-12.
4. Adamchuk, V. I.; Hummel, J. W.; Morgan, M. T.; Upadhyaya, S. K. On-The-Go Soil Sensors for Precision Agriculture. *Comput. Electron. Agr.* **2004**, *44*, 71-91.
5. Ali, M. A.; Jiang, H.; Mahal, N.K.; Weber, R.J.; Kumar, R.; Castellano, M.J.; Dong, L. Microfluidic Impedimetric Sensor for Soil Nitrate Detection using Graphene Oxide and Conductive Nanofibers Enabled Sensing Interface. *Sensors and Actuators B: Chemical* **2017**, 239, 1289-1299.
6. Ali, M. A.; Mondal, K.; Wang, Y.; Jiang, H.; Mahal, N. K.; Castellano, M. J.; Sharma, A.; Dong, L. In Situ Integration of Graphene Foam–Titanium Nitride based Bio-Scaffolds and Microfluidic Structures for Soil Nutrient Sensors. *Lab Chip* **2017**, *17*, 274-85.
7. Dalal, R. C.; Henry, R. J. Simultaneous Determination of Moisture, Organic Carbon, and Total Nitrogen by Near Infrared Reflectance Spectrophotometry. *S. S. S. A.* **1986**, *50*, 120-3.
8. Hood-Nowotny, R.; Umana, N. H.; Inselbacher, E.; Oswald-Lachouani, P.; Wanek, W. Alternative methods for measuring inorganic, organic, and total dissolved nitrogen in soil. *Soil Sci. Soc. Am. J.* **2010**, *74*, 1018-27.
9. Daniel, A.; Birot, D.; Lehaitre, M.; Poncin, J. Characterization and reduction of interferences in flow-injection analysis for the in situ determination of nitrate and nitrite in sea water. *Anal. Chim. Acta* **1995**, *308*, 413-24.
10. Schroeder, D. C.; The analysis of nitrate in environmental samples by reversed-phase HPLC. *J. Chromatogr. Sci.* **1987**, *25*, 405-8.
11. Yoshizumi, K.; Aoki, K.; Matsuoka, T.; Asakura, S. Determination of nitrate by a flow system with a chemiluminescent nitrogen oxide (NOx) analyzer. *Anal. Chem*. **1985**, *57*, 737-40.
12. Englmaier, P. Nitrate analysis by gas-liquid chromatography using the nitration of 2, 4-dimethylphenol in sulphuric acid. *J. Chromatogr. A* **1983**, *270*, 243-51.
13. Zhang, C.; Kovacs, J. M. The Application of Small Unmanned Aerial Systems for Precision Agriculture: A Review. *Precis. Agric.* **2012**, *13*, 693-712.

14. Mills, H. A.; Jones, Jr J. B. Nutrient Deficiencies and Toxicities in Plants: Nitrogen. *J. Plant Nutr. Soil. Sci.* **1979**, *1*, 101-22.
15. Ali, Md. A.; Hong, W.; Oren, S.; Wang, Q.; Wang, Y.; Jiang, H.; Dong, L. Tunable Bioelectrodes with Wrinkled-Ridged Graphene Oxide Surfaces for Electrochemical Nitrate Sensors. *RSC Adv.* **2016**, *6*, 67184-67195.
16. Schazmann, B.; Diamond, D. Improved Nitrate Sensing using Ion Selective Electrodes based on Urea–Calixarene Ionophores. *New J. Chem.* **2007**, *31*, 587-92.
17. Jiang, H.; Ali, Md. A.; Jiao, Y.; Yang, B.; Dong, L. In-situ, Real-time Monitoring of Nutrient Uptake on Plant Chip Integrated with Nutrient Sensor. In Proceedings of the 2017 19th International Conference on Solid-State Sensors, Actuators and Microsystems (TRANSDUCERS), Kaohsiung, Taiwan. ***2017***, pp 289–292 (IEEE).
18. Xu, Z.; Wang, X.; Weber, R. J.; Kumar, R.; Dong, L. Nutrient Sensing using Chip Scale Electrophoresis and In situ Soil Solution Extraction. *IEEE Sens. J.* **2017**, *17*, 4330-9.
19. Bobacka, J. Potential Stability of All-Solid-State Ion-Selective Electrodes using Conducting Polymers as Ion-to-Electron Transducers. *Anal. Chem.* **1999**, *71*, 4932.
20. Cattrall, R. W.; Freiser, H. Coated Wire Ion-Selective Electrodes. *Anal. Chem.* **1971**, *43*, 1905–1906.
21. Bobacka, J.; Ivaska, A.; Lewenstam, A. Potentiometric Ion Sensors. *Chem. Rev.* **2008**, *108*, 329-51.
22. Silvester, D. S. Recent Advances in the Use of Ionic Liquids for Electrochemical Sensing. *Analyst* **2011**, *136*, 4871-82.
23. Hu, J.; Andreas, S.; Philippe, B. Rational Design of All-Solid-State Ion-Selective Electrodes and Reference Electrodes. *Trends Anal. Chem.* **2016**, *76*, 102-114.
24. Cadogan, A.; Gao, Z.; Lewenstam, A.; Ivaska, A. Diamond, D. All-Solid-State Sodium-Selective Electrode based on a Calixarene Ionophore in a Poly (Vinyl Chloride) Membrane with a Polypyrrole Solid Contact. *Anal. Chem.* **1992**, *64*, 2496-501.
25. McQuade, D. T.; Pullen, A. E.; Swager, T. M. Conjugated Polymer-based Chemical Sensors. *Chem. Rev.* **2000**, *100*, 2537-74.
26. Lindner, E.; Gyurcsányi, R. E. Quality Control Criteria for Solid-Contact, Solvent Polymeric Membrane Ion-Selective Electrodes. *J. Solid State Electrochem.* **2009**, *13*, 51-68.

27. Si, P.; Bakker, E. Thin Layer Electrochemical Extraction of Non-Redoxactive Cations with an Anion-Exchanging Conducting Polymer Overlaid with a Selective Membrane. *Chem. Comm.* **2009**, 5260-2.
28. Vázquez, M.; Bobacka, J.; Ivaska, A. Potentiometric Sensors for Ag+ based on Poly (3-Octylthiophene)(POT). *J. Solid State Electrochem.* **2005**, *9*, 865-73.
29. Gao, W.; Emaminejad, S.; Nyein, H. Y.; Challa, S.; Chen, K.; Peck, A.; Fahad, H. M.; Ota, H.; Shiraki, H.; Kiriya, D.; Lien, D. H. Fully Integrated Wearable Sensor Arrays for Multiplexed in situ Perspiration Analysis. *Nature* **2016,** *529*, 509-514.
30. Bobacka, J. Potential Stability of All-Solid-State Ion-Selective Electrodes using Conducting Polymers as Ion-to-Electron Transducers. *Anal. Chem.* **1999**, *71*, 4932-7.
31. Fibbioli, M.; Morf, W. E.; Badertscher, M.; de Rooij N. F.; Pretsch, E. Potential Drifts of Solid-Contacted Ion-Selective Electrodes due to Zero-Current Ion Fluxes Through the Sensor Membrane. *Electroanalysis* **2000**, *12*, 1286-92.
32. Ping, J.; Wang, Y.; Wu, J.; Ying, Y. Development of an All-Solid-State Potassium Ion-Selective Electrode using Graphene as the Solid-Contact Transducer. *Electrochem. Commun.* **2011**, *13*, 1529-32.
33. Anastasova-Ivanova, S.; Mattinen, U.; Radu, A.; Bobacka, J.; Lewenstam, A.; Migdalski, J.; Danielewski, M.; Diamond, D. Development of Miniature All-Solid-State Potentiometric Sensing System. *Sens. Actuators B Chem.* **2010**, *146*, 199-205.
34. Dam, V. A.; Zevenbergen, M. A.; Van Schaijk, R. Toward Wearable Patch for Sweat Analysis. *Sens. Actuators B Chem.* **2016**, *236*, 834-8.
35. Athavale, R.; Dinkel, C.; Wehrli, B.; Bakker, E.; Crespo, G. A.; Brand, A. Robust Solid-Contact Ion Selective Slectrodes for High-Resolution in situ Measurements in Fresh Water Systems. *Environ. Sci. Technol. Lett.* **2017**, *4*, 286-91.
36. Yuan, D.; Anthis, A. H.; Ghahraman, A. M.; Pankratova, N.; Cuartero, M.; Crespo, G. A.; Bakker, E. All-Solid-State Potentiometric Sensors with a Multiwalled Carbon Nanotube Inner Transducing Layer for Anion Detection in Environmental Samples. *Anal. Chem.* **2015**, *87*, 8640-5.
37. Zhu, J.; Li, X.; Qin, Y.; Zhang, Y. Single-Piece Solid-Sontact Ion-Selective Electrodes with Polymer–Carbon Nanotube Composites. *Sens. Actuators B Chem.* **2010**, *148*, 166-72.

38. Criscuolo, F.; Taurino, I.; Stradolini, F.; Carrara, S.; De Micheli, G. Highly-Stable Li+ Ion-Selective Electrodes based on Noble Metal Nanostructured Layers as Solid-Contacts. *Anal. Chim. Acta* **2018**, *1027*, 22-32.

39. Lai, C. Z.; Fierke, M. A.; Stein, A.; Bühlmann, P. Ion-Selective Electrodes with Three-Dimensionally Ordered Macroporous Carbon as the Solid Contact. *Anal. Chem.* **2007**, *79*, 4621-6.

40. Bobacka, J. Conducting Polymer-based Solid-State Ion-Selective Electrodes. *Electroanalysis* **2006**, 18, 7-18.

41. Guo, J.; Amemiya, S. Voltammetric Heparin-Selective Electrode based on Thin Liquid Membrane with Conducting Polymer-Modified Solid Support. *Anal. Chem.* **2006**, *78*, 6893-902.

42. Kim, Y.; Amemiya, S. Stripping Analysis of Nanomolar Perchlorate in Drinking Water with a Voltammetric Ion-Selective Electrode based on Thin-Layer Liquid Membrane. *Anal. Chem.* **2008**, *80*, 6056-65.

43. Veder, J. P.; De Marco, R.; Clarke, G.; Chester, R.; Nelson, A.; Prince, K.; Pretsch, E.; Bakker, E.; Elimination of Undesirable Water Layers in Solid-Contact Polymeric Ion-Selective Electrodes. *Anal. Chem.* **2008**, *80*, 6731-40.

44. Silva, E. A.; Oliveira, V. J.; Braunger, M. L.; Constantino, C. J.; Olivati, C. D. Poly (3-Octylthiophene)/Stearic Acid Langmuir and Langmuir-Blodgett Films: Preparation and Characterization. *Mat. Res.* **2014**, *17*, 1442-8.

45. Jarvis, J. M.; Guzinski, M.; Pendley, B. D.; Lindner, E.; Poly(3-Octylthiophene) as Solid Contact for Ion-Selective Electrodes: Contradictions and Possibilities. *J. Solid State Electrochem.* **2016**, *20*, 3033–3041.

46. Yang, L.; Wang, S.; Mao, J.; Deng, J.; Gao, Q.; Tang, Y.; Schmidt, O. G. Hierarchical MoS_2/Polyaniline Nanowires with Excellent Electrochemical Performance for Lithium-Ion Batteries. *Adv. Mater.* **2013**, *25*, 1180-4.

47. El Beqqali, O.; Zorkani, I.; Rogemond, F.; Chermette, H.; Chaabane, R. B.; Gamoudi, M.; Guillaud, G. Electrical Properties of Molybdenum Disulfide MoS_2. Experimental Study and Density Functional Calculation Results. *Synth. Met.* **1997**, *90*, 165-72.

48. Wu, S.; Zeng, Z.; He, Q.; Wang, Z.; Wang, S. J.; Du, Y.; Yin, Z.; Sun, X.; Chen, W.; Zhang, H. Electrochemically Reduced Single-Layer MoS_2 Nanosheets: Characterization, Properties, and Sensing Applications. *Small* **2012**, *8*, 2264-70.
49. Barua, S.; Dutta, H. S.; Gogoi, S.; Devi, R.; Khan, R. Nanostructured MoS_2-Based Advanced Biosensors: A Review. *ACS Appl. Bio Mater*. **2018**, *1*, 2-5.
50. Yang, T.; Meng, L.; Chen, H.; Luo, S.; Li, W.; Jiao, K. Synthesis of Thin-Layered Molybdenum Disulfide-based Polyaniline Nanointerfaces for Enhanced Direct Electrochemical DNA Detection. *Adv. Mater. Interfaces* **2016**, *3*, 1500700.
51. Wang, J.; Wu, Z.; Yin, H.; Li, W.; Jiang, Y. Poly (3, 4-ethylenedioxythiophene)/MoS_2 Nanocomposites with Enhanced Electrochemical Capacitance Performance. *RSC Adv.* **2014**, *4*, 56926-32.
52. Jang, A.; Zou, Z.; Lee, K. K.; Ahn, C. H.; Bishop, P. L. Potentiometric and Voltammetric Polymer Lab Chip Sensors for Determination of Nitrate, pH and Cd (II) in Water. *Talanta* **2010**, *83*, 1-8.
53. Nolan, M. A.; Tan, S. H.; Kounaves, S. P. Fabrication and Characterization of a Solid State Reference Electrode for Electroanalysis of Natural Waters with Ultramicroelectrodes. *Anal. Chem.* **1997**, *69*, 1244-7.
54. Bates, R. G. Macaskill, J. B. Standard Potential of the Silver-Silver Chloride Electrode. *Pure Appl. Chem.* **1978**, *50*, 1701-6.
55. Bakker, E.; Pretsch, E. Potentiometric Sensors for Trace-Level Analysis. *Trends Anal. Chem.* **2005**, *24*, 199-207.
56. Bakker, E. Selectivity of Carrier-based Ion-Selective Electrodes: is the Problem Solved?. *Trends Anal. Chem.* **1997**, *16*, 252-60.
57. Baker, M. A.; Gilmore, R.; Lenardi, C.; Gissler, W. XPS Investigation of Preferential Sputtering of S from MoS_2 and Determination of MoSx Stoichiometry from Mo and S peak Positions. *Appl. Surf. Sci.* **1999**, *150*, 255-62.
58. Wang, F.; Mori, K.; Oishi, Y. Electrochemical Polymerization of 6-(N-allyl-1, 1, 2, 2-Tetrahydroperfluorodecyl) Amino-1, 3, 5-Triazine-2, 4-Dithiol Monosodium on Aluminum. *Polym. J.* **2006**, *38*, 484.
59. Buck, R. P.; Lindner, E. Recommendations for Nomenclature of Ionselective Electrodes (IUPAC Recommendations 1994). *Pure Appl. Chem.* **1994**, *66*, 2527-36.

60. Cuartero, M.; Crespo, G. A.; Bakker, E. Tandem Electrochemical Desalination–Potentiometric Nitrate Sensing for Seawater Analysis. *Anal. Chem.* **2015**, *87*, 8084-9.
61. Bendikov, T. A.; Kim, J.; Harmon, T. C. Development and Environmental Application of a Nitrate Selective Microsensor based on Doped Polypyrrole Films. *Sens. Actuators B Chem.* **2005**, *106*, 512-7.
62. Garland, N. T.; McLamore, E. S.; Cavallaro, N. D.; Mendivelso-Perez, D.; Smith, E. A.; Jing, D.; Claussen, J. C. Flexible Laser-Induced Graphene for Nitrogen Sensing in Soil. *ACS Appl. Mater. Interfaces* **2018**, *10*, 39124-33.
63. Chaneam, S.; Taweetong, W.; Kaewyai, K.; Thienwong, P.; Takaew, A.; Chaisuksant, R. Fabrication of a Nitrate Selective Electrode for Determination of Nitrate in Fertilizers by using Flow Injection Analysis System. *Procedia Chem.* **2016**, *20*, 73-5.
64. Khripoun, G. A.; Volkova, E. A.; Liseenkov, A. V.; Mikhelson, K. N. Nitrate-Selective Solid Contact Electrodes with Poly (3-Octylthiophene) and Poly (aniline) as Ion-to-Electron Transducers Buffered with Electron-Ion-Exchanging Resin. *Electroanalysis* **2006**, *18*, 1322-8.
65. Rudd, S.; Dalton, M.; Buss, P.; Treijs, A.; Portmann, M.; Ktoris, N.; Evans, D. Selective Uptake and Sensing of Nitrate in Poly (3, 4-ethylenedioxythiophene). *Sci. Rep.* **2017**, *29*, 16581.
66. Wardak, C. Solid Contact Nitrate Ion-Selective Electrode Based on Ionic Liquid with Stable and Reproducible Potential. *Electroanalysis* **2014**, *26*, 864-72.
67. Pięk, M.; Piech, R.; Paczosa-Bator, B. All-solid-state nitrate selective electrode with graphene/tetrathiafulvalene nanocomposite as high redox and double layer capacitance solid contact. *Electrochim. Acta* **2016**, *210*, 407-14.
68. Paczosa-Bator, B. Effects of type of nanosized carbon black on the performance of an all-solid-state potentiometric electrode for nitrate. *Microchim. Acta* **2014**, *181*, 1093-9.
69. Pięk, M.; Piech, R.; Paczosa-Bator, B. Improved nitrate sensing using solid contact ion selective electrodes based on TTF and its radical salt. *J. Electrochem. Soc.* **2015**, *162*, B257-63.

70. Umezawa, Y.; Bühlmann, P.; Umezawa, K.; Tohda, K.; Amemiya, S. Potentiometric Selectivity Coefficients of Ion-Selective Electrodes. Part I. Inorganic cations (technical report). *Pure Appl. Chem*. **2000**, *72*, 1851-2082.

71. Nägele, M.; Bakker, E.; Pretsch, E. General Description of the Simultaneous Response of Potentiometric Ionophore-based Sensors to Ions of Different Charge. *Anal. Chem.* **1999**, *71*, 1041-1048.

Table of Contents graphic